# Properties of amorphous GaN from first-principles simulations

B. Cai and D. A. Drabold
*Department of Physics and Astronomy, Ohio University, Athens, Ohio 45701, USA*
(Received 8 March 2011; revised manuscript received 18 July 2011; published 15 August 2011)

Amorphous GaN (a-GaN) models are obtained from first-principles simulations. We compare four a-GaN models generated by "melt-and-quench" and the computer alchemy method. We find that most atoms tend to be fourfold, and a chemically ordered continuous random network is the ideal structure for a-GaN albeit with some coordination defects. Where the electronic structure is concerned, the gap is predicted to be less than 1.0 eV, underestimated as usual by a density functional calculation. We observe a highly localized valence tail and a remarkably delocalized exponential conduction tail in all models generated. Based upon these results, we speculate on potential differences in *n*- and *p*-type doping. The structural origin of tail and defect states is discussed. The vibrational density of states and dielectric function are computed and seem consistent with experiment.

DOI: 10.1103/PhysRevB.84.075216 PACS number(s): 61.43.Bn, 61.43.Dq, 71.23.An

## I. INTRODUCTION

With a profound impact on lighting technology and other applications, crystalline GaN has been the subject of vast inquiry.[1–3] However, lattice mismatch with substrates makes it difficult to grow. Recently, *amorphous* GaN (a-GaN) has become attractive due to its potential to solve lattice match problems and advantages accruing from its natural isotropy. A number of experiments have investigated the structural and optoelectronic properties of a-GaN.[4–9]

In 1997, Stumm and Drabold[10] reported the first a-GaN atomistic model and proposed that a-GaN might find use as an electronic material. However, there are some limitations in that work. First, the previous calculations were done with a version of FIREBALL[11] using the Harris functional local density approximation (LDA)[12] and a local basis set. Though they predicted an electronic gap close to experimental value, it is well known that the incompleteness of the basis tends to exaggerate the gap, which compensated the underestimate for the electronic gap in density functional theory. Second, to obtain the correct lattice constant, the LDA repulsive pair interaction was empirically rescaled. This paper checks the previous work and, while we find that the basic picture there was correct, we add important results with more modern techniques.

The structure of a-GaN is controversial. Some experiments observe a large concentration of homopolar bonds,[13] contradicting other studies.[8] There are no N-N or Ga-Ga bonds in Stumm's models, but other calculations suggest a more chemically disordered network.[14] Doping of a-GaN is an important topic that we do not explore, but a full understanding of the intrinsic electronic features of undoped a-GaN, like the origin of defect states and tail states, is a necessary precursor.

In this paper, we propose atomistic a-GaN models formed via *ab initio* molecular dynamics simulation with a plane-wave basis. Models are generated in different ways and compared. For all models, the network topology is analyzed through radial and angular distribution functions, and structural statistics. We find that Ga and N atoms strongly prefer to be fourfold, and homopolar bonds are rare in the network. This result indicates that Stumm's model is basically correct but with too many coordination defects (threefold atoms). The difference between the LDA and Perdew-Burke-Ernzerhof (PBE) generalized gradient approximation (GGA) methods, and different treatment for Ga 3*d* states, is also discussed. We then predict electronic properties and connect the electronic structure to the topology of the network. We show that the conduction edge has Urbach (exponential) form and is extraordinarily delocalized, and the valence edge is very sharp with highly localized states. The delocalized nature of the conduction tail is the most interesting result in this paper. Vibrational properties and dielectric functions are also predicted. Naturally, the detailed properties depend upon the mode of growth of the material; our work is most relevant to least-defective "ideal" a-GaN. Models are generated using different modeling schemes; their relative merits and value for predicting the properties of a-GaN are discussed further in the Conclusions.

## II. SIMULATION METHODS

Some elements in the periodic table, from the same group, form similar bulk structures (like Si and Ge, both forming tetrahedral structures in their amorphous phase). In this case, an initial model could be made based on previously generated models by replacing the old species with from the same column and rescaling the cell to fit the mass density and allowing for relaxation effects. For example, a-GaN could be generated by replacing As with N atoms in an a-GaAs model. This method may be called computer alchemy. We carry this method out here and also use the conventional "melt-and-quench" method to form a-GaN models.[15]

In our work, the major calculations are performed with the Vienna Ab-initio Simulation Package (VASP)[16] based on density functional theory (DFT) within the LDA[17] and Vanderbilt's ultrasoft pseudopotentials[18] in which the Ga 3*d* states are included in the core. Three models are generated via computer alchemy: a 64-atom model (64-atom model II, obtained from a 64-atom InN model of Ref. 19), the 250-atom model I (obtained from the 250-atom a-GaAs model of Ref. 20), and the 250-atom model II (obtained from the 250-atom a-InN model of Ref. 19). The 64-atom model II is annealed and equilibrated at 500 K and the 250-atom model I is annealed and equilibrated at 300 K. Furthermore, another

 

TABLE I. The statistical distribution of the main structural components of four models.

| Model | Density ($g/cm^3$) | N-N | Ga-Ga | $N_3$ | $N_4$ | $N_5$ | $Ga_3$ | $Ga_4$ | $Ga_5$ | $n_N$ | $n_{Ga}$ | $E_{tot}$/atom (eV) |
|---|---|---|---|---|---|---|---|---|---|---|---|---|
| 64-atom model I | 5.8 | 0 | 0 | 13% | 87% | 0 | 13% | 87% | 0 | 3.86 | 3.86 | −6.05 |
| 64-atom model II | 5.8 | 0 | 0 | 3% | 97% | 0 | 6% | 91% | 3% | 3.97 | 3.97 | −5.97 |
| 250-atom model I | 5.6 | 0 | 0 | 11% | 87% | 2% | 9% | 89% | 1% | 3.91 | 3.91 | −5.90 |
| 250-atom model II | 5.6 | 2% | 0 | 9% | 89% | 2% | 11% | 87% | 2% | 3.92 | 3.90 | −5.89 |
| Stumm's model | 5.0 | 0 | 0 | 69% | 31% | 0 | 63% | 37% | 0 | 3.31 | 3.37 | −5.71 |
| Relaxed Stumm's model | 5.8 | 0 | 0 | 13% | 84% | 3% | 13% | 87% | 0 | 3.90 | 3.86 | −5.87 |

64-atom model (the 64-atom model I) is generated by the melt-and-quench method: the 64-atom model II is melted at 3000 K for 10 ps, annealed to 1500 K for 40 ps, and quenched to 0 K with an average quench rate of 40 K/ps. In addition, we generated three more 64-atom computer alchemy a-GaN models with similar procedures (annealed at 500 K, quenched to 0 K, and zero pressure) but using three different methods: (1) LDA with pseudopotential including Ga 3*d* states in the core,[17,18] (2) GGA-PBE with pseudopotential including Ga 3*d* states in the core,[18,21] and (3) LDA with pseudopotential describing Ga 3*d* electrons as valence electrons.[17,18] The dynamic simulations for all models are done at the Γ point. We use 63 *k*-points for electronic density of states (EDOS) calculations in the 64-atom cell, and 8 *k*-points for EDOS calculations in the 250-atom cell.

## III. RESULTS AND DISCUSSION

### A. Structure properties

We list the major parameters of different a-GaN models in Table I. For comparison, we also calculated the total energy for Stumm's model by VASP and relaxed it. After zero-pressure relaxation, the density of both 64-atom models are close to 5.8 $g/cm^3$, 95% of the experimental WZ-GaN density (6.06 $g/cm^3$)[22]; both 250-atom models have mass densities around 5.6 $g/cm^3$, 92% of the experimental WZ-GaN density. Where chemical order is concerned, there are no homopolar bonds in either the 64-atom models or the 250-atom model I, and there is only one N-N bond in the 250-atom model II as one might expect for a significantly ionic system.

Where coordination is concerned, most atoms tend to be fourfold, suggesting that a-GaN retains the zinc-blende/wurtzite character of crystalline GaN, in significant contrast to Stumm's model. The 64-atom computer alchemy model (64-atom model II) predicts more fourfold atoms than the melt-and-quench model (64-atom model I). Considering the energy, the 64-atom model I gives the best cohesive energy, followed by the 64-atom model II. Both the new 64-atom models show much lower cohesive energy (lower by 0.34 and 0.26 eV/atom) compared to the original Stumm model. Both 250-atom models show a slightly higher energy compared to the 64-atom models, and the increased cohesive energy in 250-atom model II is likely due to the N-N bond. We also notice that if relaxed with VASP, most atoms in Stumm's model become fourfold with a reduced total energy. These results suggest that an ideal a-GaN is a chemically ordered continuous random network with most but *not* all atoms being fourfold. The computer alchemy method suggests an upper-limit number of fourfold atoms in the network and the original Stumm model contains too many threefold atoms according to VASP.

To further analyze the network, we plot the partial pair-correlation functions of the four models in Fig. 1. For the Ga-N partial, there exists a sharp first peak around 1.94 Å and all four models show similar features. For both N-N and Ga-Ga partials, the melt-and-quench model shows a higher principal peak around 3.1 Å. Particularly for the Ga-Ga partial, computer alchemy models have a prepeak or shoulder around 2.7 Å (marked by a black arrow), which is not observed in the melt-and-quench model. The following analysis on angle distributions proves that these peaks are related to edge-sharing tetrahedral structures. Due to the N-N bond, there is a small peak around 1.53 Å in the N-N partial of the 250-atom model II (marked by a black arrow). Overall, the pair-correlation functions of four models exhibit similar features.

Next, we analyze the angle distributions for Ga-N-Ga bonds and N-Ga-N bonds. The 250-atom models yield major peak positions close to $\theta_T = 109.47^\circ$ for both Ga-N-Ga and

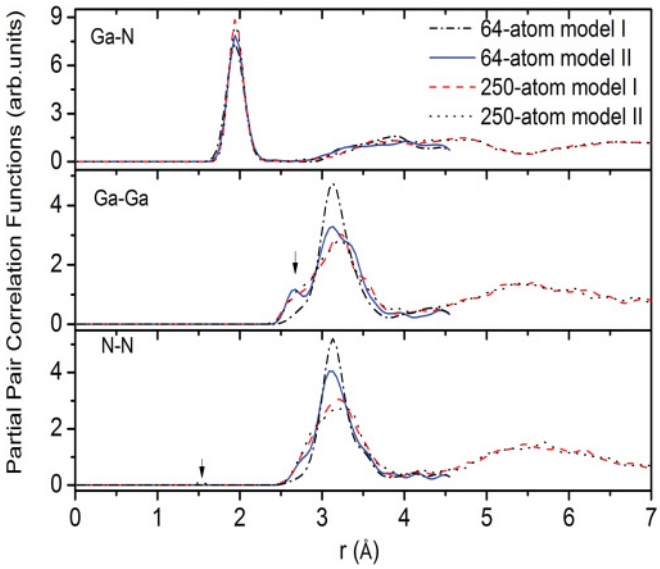


FIG. 1. (Color online) Partial pair correlation functions of the three models (see text). In the Ga-Ga partial, the prepeak and shoulders are marked by a black arrow. For the N-N partial, the black arrow marks the peak due to the only N-N bond in the 250-atom model II.

TABLE II. The statistical distribution of the main structural components of four models.

| Model | Lattice constant (Å) | N-N | Ga-Ga | $N_3$ | $N_4$ | $Ga_3$ | $Ga_4$ | $Ga_5$ | $n_N$ | $n_{Ga}$ |
|---|---|---|---|---|---|---|---|---|---|---|
| LDA (3*d* in core) | 9.14 | 0 | 0 | 3% | 97% | 6% | 91% | 3% | 3.97 | 3.97 |
| GGA (3*d* in core) | 9.28 | 0 | 0 | 3% | 97% | 6% | 91% | 3% | 3.97 | 3.97 |
| LDA (3*d* in valence) | 9.23 | 0 | 0 | 9% | 91% | 9% | 91% | 0 | 3.91 | 3.91 |

N-Ga-N angles. The 64-atom melt-and-quench model has very sharp major peaks around $\theta_T$ in both Ga-N-Ga and N-Ga-N distributions. Though the major peak positions are slightly off $\theta_T$ for the 64-atom computer alchemy model, the mean value of N-Ga-N and Ga-N-Ga angles are 109.15° and 108.65°, respectively, which are still close to $\theta_T$. Thus, we conclude that a-GaN retains strong vestiges of its crystalline short-range order and tends to form a tetrahedral structure. We observe prepeaks or shoulders around 80° for all the computer alchemy models in the Ga-N-Ga angle distribution, which implies that there are two distinct sites for Ga atoms in these models. We find that the small angle is due to edge-sharing units with distorted angles (appearing as four-member rings with the Ga-N-Ga angle between 75° and 95°). We show that this kind of distortion is responsible for some of the electronic tail states.

Finally for this section, we show comparisons among three models generated by different ultrasoft pseudopotentials and density functionals. This includes LDA, and GGA with Ga 3*d* states in the core and as valence states. The statistics obtained from these models are list in Table II and the bond-length distributions are plotted in Fig. 2. The LDA and GGA methods predict the same mean coordination numbers and the same amount of $N_3$, $N_4$, $Ga_3$, and $Ga_4$ units. The only difference is that the GGA predicts a slightly bigger cell and a longer averaged bond length, as expected. The major peak in bond-length distribution is shifted to 1.96 Å for GGA compared with 1.93 Å for LDA. The partial pair-correlation functions of both LDA and GGA models show the same features with slightly shifted peak positions (not plotted here). When Ga 3*d* states are treated as valence electrons, the fraction of threefold atoms is slightly increased. The peak position of the bond-length distribution is around 1.96 Å. Since the experimental value of the Ga-N bond length is around 1.95 Å,[22,23] there is no significant difference between the network obtained by LDA and GGA methods and the different treatment of Ga 3*d* states.

### B. Vibrational properties

The vibrational properties of a-GaN are reported through the vibrational density of states (VDOS). Starting with a thoroughly relaxed cell, the force constant and dynamical matrix is obtained from perturbing each atom in turn by 0.015 Å and computing forces on all atoms in the model for each perturbed conformation. The VDOS of the 64-atom melt-and-quench model and the 250-atom model II are reported in Fig. 3. Both models show similar features. For comparison, we also plot the VDOS of crystalline GaN from Ref. 24 as an inset. Our results show that the amorphous VDOS retains some features of the crystalline VDOS, such as the two peaks in the first band. However, we did not observe two distinguished peaks in the optical band,[25] and the gap between the acoustic band and the optical band fills in substantially. The results are quite consistent with a recent Raman study.[8]

### C. Electronic structure

We describe the electronic structure by analyzing the EDOS, the inverse participation ratio (IPR or $\mathcal{I}$) of the individual states, and dielectric functions. Figure 4 shows the EDOS of the four models. Overall, all EDOS have similar

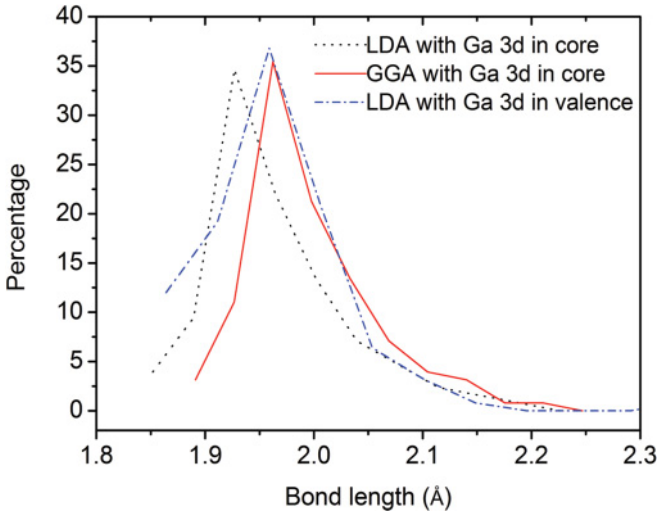


FIG. 2. (Color online) Comparison of bond-length distributions for three computer alchemy models generated with different ultrasoft pseudopotentials and density functionals.

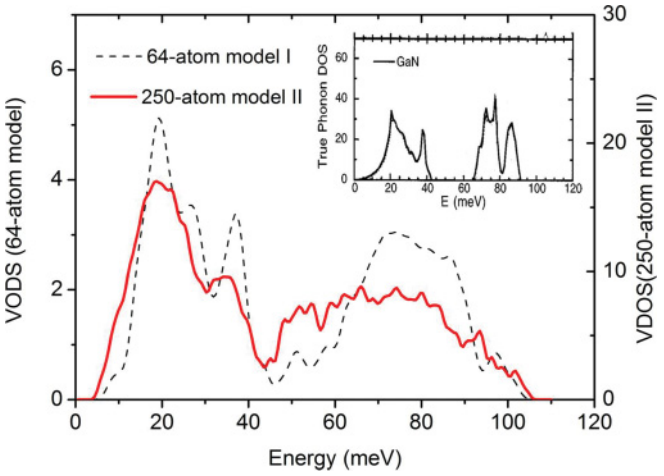


FIG. 3. (Color online) Vibrational density of states of the 64-atom model and the 250-atom model II. The eigenvalues were Gaussian broadened with a width of 1 meV. The VDOS of crystal wurtzite GaN is plotted as an inset from Ref. 24.

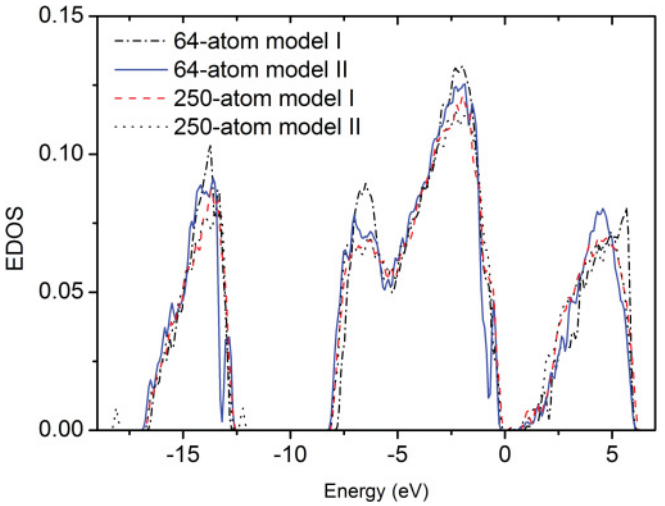


FIG. 4. (Color online) Electronic density of states of the 64-atom models (63 $k$-points are used) and 250-atom models (8 $k$-points are used) obtained by LDA and ultrasoft pseudopotential with a Ga 3$d$ electron in the core. The Fermi level is at 0 eV.

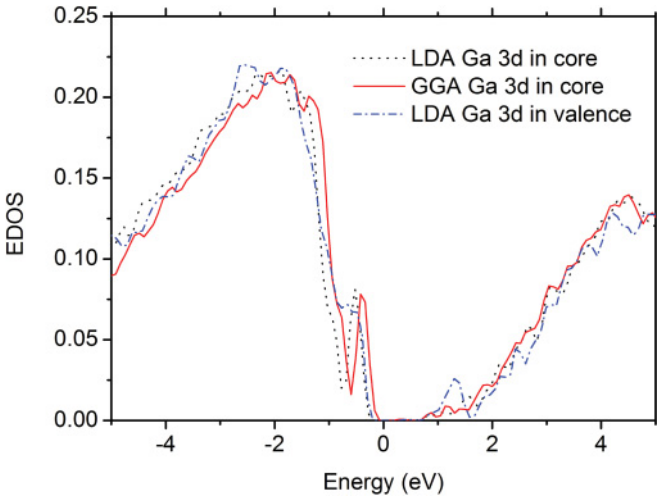


FIG. 5. (Color online) EDOS around the band gap of the 64-atom computer alchemy models generated by different ultrasoft pseudopotentials and density functionals: LDA with Ga 3$d$ states in the core, GGA with Ga 3$d$ states in the core, and LDA with Ga 3$d$ states in valence. The Fermi level is at 0 eV.

characters with slight differences in detail. The valence-band tails are very sharp, and shallow valence states are observed in all models (a peak in the valence tail of the 64-atom model II and shoulders in the valence tail of 64-atom model I, 250-atom model I, and 250-atom model II). We show later that these tail states are associated with threefold N atoms. The conduction-band tail is *dramatically* broader and consists of essentially extended states in stark contrast with the valence tail for a system like a-Si.[26] By fitting the conduction-band tail to an exponential, we report the Urbach energy, $E_u \approx 410$ meV for the 64-atom model I, $E_u \approx 420$ meV for the 64-atom model II, and $E_u \approx 490$ meV for the 250-atom model I, comparable to the reported value of "several hundred meV" in Ref. 27. In addition, for the 250-atom model II, there are defect states in the deep band region between $-18$ and $-12$ eV, far below the Fermi level. These states are due primarily to the N-N bond. We did not observe any electronic signature of the N-N bond around the optical gap. If we define the band gap as the difference between the highest occupied molecular orbital (HOMO) and the lowest unoccupied molecular orbital (LUMO) based on the $\Gamma$ point, then the magnitude of the electronic gap is 1.10 eV for the 64-atom model I, 1.00 eV for the 64-atom model II, 0.69 eV for the 250-atom model I, and 0.71 eV for the 250-atom model II. The band gaps obtained from our models are much smaller than the experimental value of 3.1 eV.[7] This is not a surprising result, since DFT always underestimates the gap.[28] If we estimate the mobility gap (the gap between extended valence and conduction states), we obtain $E_g \approx 3.0$ eV.

In Fig. 5, we show the EDOS around the band gap based on the 64-atom computer alchemy models generated by different pseudopotentials and density functionals: LDA (Ga 3$d$ states in the core), GGA (Ga 3$d$ states in the core), and LDA (Ga 3$d$ states in valence). We could see that the EDOS from LDA and GGA methods with Ga 3$d$ states in the core are almost identical. When Ga 3$d$ states are treated as valence, the conduction tail is slightly different: more tail states are observed. But the band gap is almost the same. Thus, we conclude that LDA and GGA methods predict similar EDOS around the band gap, and the Ga 3$d$ states have some impact on the conduction tail.

To characterize the localization of the tail states around the gap, we performed an IPR ($\mathcal{I}$) analysis for all four models. The $\mathcal{I}$ measures the degree of localization given an electronic state.[29] For highly localized states, $\mathcal{I} = 1$; for extended states, $\mathcal{I} = 1/N$, where $N$ is the number of atoms. The results are plotted in Fig. 6. For all models, the valence tail states exhibit much higher $\mathcal{I}$, indicating a high localization in contrast to the conduction tail which consists of more extended states. The 64-atom model I shows fewer highly localized tail states than computer alchemy models.

By projecting the EDOS onto different atomic orbitals, we find that the valence tail is built from N $p$, Ga $p$, and Ga $d$ orbitals. This implies a high sensitivity to bond-angle disorder,

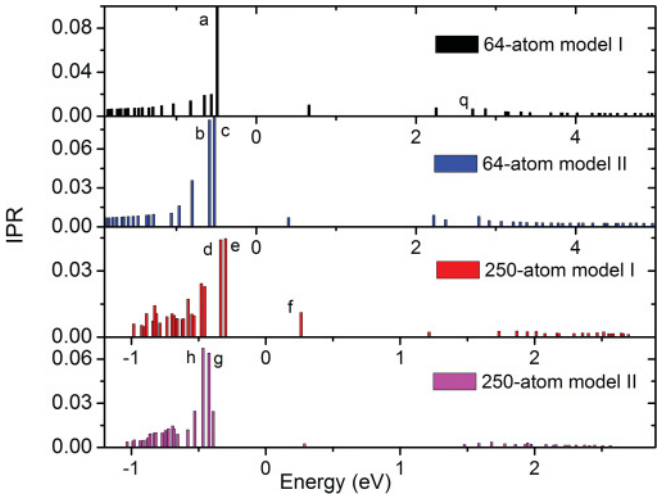


FIG. 6. (Color online) Inverse participation ratio analysis for four models. Large IPR implies strong localization. Note the highly delocalized conduction tail. The Fermi level is at 0 eV.

which is presumably the reason for high localization. The conduction tail is localized on *both* Ga *s* and N *s* orbitals. Since the *s*-*s* interaction is *only* affected by bond length, which is very close to a fixed value in this system, the conduction-tail states exhibit remarkably weak localization and the conduction tail is almost immune to angle disorder. This situation is somewhat analogous to amorphous oxides, like a-$SiO_2$, a-$SnO_2$, and a-$In_2O_3$, where there is also a large asymmetry on IPR between valence-band and conduction-band tails, as discussed by Robertson[30] and in other papers.[31] However, in those oxides, the conduction-tail states mostly reside on metal *s* states, which are only affected by the second-neighbor distance of metal atoms. Thus, the reason for the large asymmetry in our system and oxides is different. To our knowledge, this effect has not been reported in nitrides until now. The asymmetry in width and localization of tail states suggests that *n* and *p* doping for a-GaN would be quite different.[32] Due to the highly localized valence-band tail states, it would be more difficult to move the Fermi level toward the valence mobility edge, complex compensations may occur, and mobility is likely to be very poor. Thus, the practical *p*-type doping is expected to be much more difficult than *n*-type doping to obtain the same carrier concentration.[33] High electron mobilities are expected, *if* the material can be *n*-type doped.

To correlate electronic structure with topological units, we picked seven electronic states (*a*–*h* in Fig. 6) with relatively high IPR and projected them onto individual atom sites. In Fig. 7, we present the characteristic atomic sites associated with tail states *a*–*h*. In the 64-atom model I, the valence tail state *a* is associated with threefold N atom 25 [Fig. 7(a)]. For the 64-atom model II, tail states *b* and *c* are highly localized on atom 13 [Fig. 7(b)], whose four neighbors are almost in the same plane, with distorted Ga-N-Ga angle 75°; state *c* is also localized on atom 28 [Fig. 7(c)], the only threefold N atom in

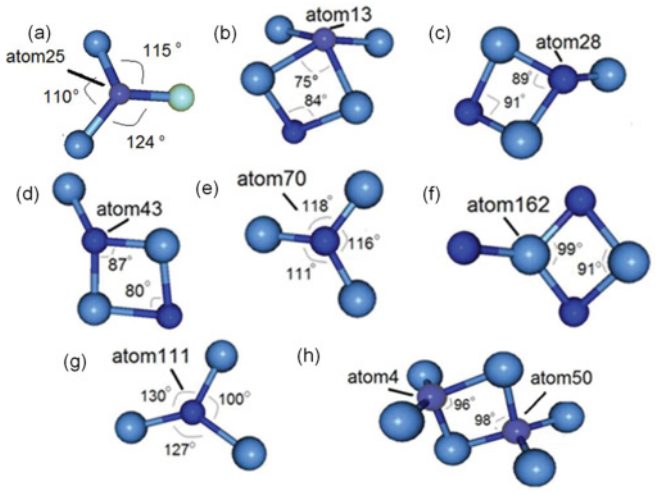


FIG. 7. (Color online) Atomistic origin of electronic tail and gap states correlated with states *a*–*h* indicated in Fig. 6. Dark (small) atoms are N; light (large) atoms are Ga: (a) atom 25 is associated with tail states *a*, (b) atom 13 is associated with tail states *b* and *c*, (c) atom 28 is associated with tail state *c*, (d) atom 43 is associated with tail states *d* and *e*, (e) atom 70 is associated with tail state *e*, (f) atom 162 is associated with tail state *f*, (g) atom 111 is associated with tail state *g*, and (h) atom 4 and atom 50 are associated with tail state *h*.

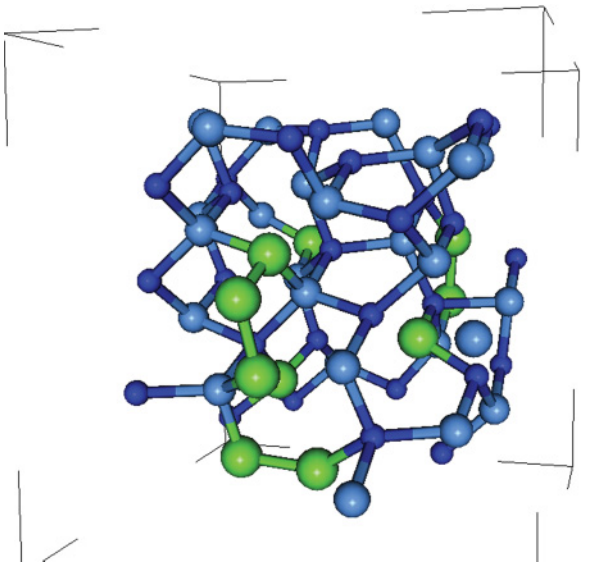

FIG. 8. (Color online) Delocalization of conduction-band tail state *q* in Fig. 6 of the 64-atom model I. Atoms contributing most to the conduction band tail (either Ga or N) are marked as green (large light grey atoms). The light blue (medium sized grey atoms) are Ga atoms and the dark blue (small dark atoms) are N atoms. Note the pattern of delocalization is filamentary as discussed in Ref. 26.

the network which formed a small Ga-N-Ga angle near 89°. In the 250-atom model I, threefold N atom 43 [Fig. 7(d)], which formed an 87° Ga-N-Ga angle, is strongly associated with eigenstates *d* and *e*; tail state *d* is also localized on atom 70 [Fig. 7(e)], a threefold N atom with all its neighbors almost in the same plane. Moreover, the conduction-band tail state *f* is mainly localized on atom 162 [Fig. 7(f)], a threefold Ga atom with disordered N-Ga-N angle. In the 250-atom model II, the threefold N atom 111, whose three neighbors are almost in the same plane [Fig. 7(g)], contributes more to valance-band tail state *g*; two fourfold N atoms, atom 4 and atom 50, forming an edge-shared tetrahedron with disordered Ga-N-Ga angle, are strongly associated with electronic state *h*. Overall, threefold N atoms with distorted angles are associated with valence tail states. In Fig. 8, we show an example of delocalization of the conduction-band tail state *q* in Fig. 6 of the 64-atom model I. The representative conduction-band tail state *q* is spread out over many atoms, leading to a small IPR. This is very different from amorphous column IV materials[26] or chalcogenide glasses,[34] which exhibit substantial electron localization in both band tails.

Finally, we briefly remark that, for the 64-atom model, the imaginary part of the dielectric function $\epsilon(\omega)$ has a major peak position around 6.8 eV for all three directions. This result is comparable to the experimental work reported in Ref. 9.

## IV. CONCLUSIONS

In this paper, we have considered models made in two ways: the conventional melt-and-quench method, and computer alchemy. It is to be admitted that the alchemy method is not predictive; rather it imposes a prior belief that the network should be a chemically ordered continuous random network. This is a possible limiting case for the structure, and fits with

the guesses of workers used to materials like amorphous silica or chalcogenide glasses. Nevertheless, to be very clear, it is an assumption only. To probe the question more closely, we carried out complementary melt-and-quench simulations, which are free of a preexisting bias toward a particular network, although such simulations often suffer from the limitation of freezing in too much disorder.[34] With both classes of simulations available, the net conclusion is that homopolar bonds are rare, and coordination defects (departures from the 8N rule) do occur. Because of small system sizes, especially for the melt-and-quench model, it is not possible to indicate the precise fraction of three- or fivefold N or Ga, but such odd coordination appears to be significantly rarer than in the work of Stumm and Drabold.[10] Physical observables, especially the electronic density of states and electronic localization, are quite insensitive to the topological variation among models.

In conclusion, we created four a-GaN atomistic models using current methods. Most atoms in the network tend to be fourfold and form tetrahedral structures. The "melt-and-quench" model has a lower cohesive energy, relatively bigger HOMO-LUMO gap, and fewer tail states. Computer alchemy is a quick and effective method to generate large atomistic models but in this case freezing into too much order. The GGA predicts a similar network compared with LDA but with an increased lattice constant and average bond length. In our calculation, describing Ga 3*d* states as valence has limited impact on bonding. All of the methods predict a similar EDOS around the band gap. We find an interesting and large asymmetry in localization between the valence and conduction tail due to the different orbital interaction, which should yield quite distinct properties in *n*- and *p*-type doping. This result appears to be robust with respect to all approximations explored. The atomistic origin of tail and defect states is discussed, and the disorder in bond angle is likely to introduce valence tail states, whereas the conduction tail is due primarily to bond-length disorder. The vibrational density of states retains some qualitative features from the crystal, and the dielectric functions show a peak around 6.8 eV, both of which are in agreement with experiment. Our work focuses primarily on "ideal" GaN to establish a reference model. Ion-bombarded samples are indeed likely to exhibit far more disorder.[13,14]

## ACKNOWLEDGMENTS

We thank the National Science Foundation for support under Grant No. DMR-09-03225. This work was supported in part by an allocation of computing time from the Ohio Supercomputer Center. We thank Prof. Martin Kordesch for many discussions and suggestions.

[1] S. J. Pearton, F. Ren, A. P. Zhang, and K. P. Lee, Mater. Sci. Eng. R **30**, 55 (2000).
[2] Z. X. Zhang, X. J. Pan, T. Wang, E. Q. Xie, and L. Jia, J. Alloys Compd. **467**, 61 (2009).
[3] S. J. Pearton and F. Ren, Adv. Mater. **12**, 21 (2000).
[4] T. Hariu, T. Usuba, H. Adachi, and Y. Shibata, Appl. Phys. Lett. **32**, 252 (1978).
[5] Z. Hassan, M. E. Kordesch, W. M. Jadwisienzak, H. Lozykowski, W. Halverson, and P. C. Colter, Mat. Res. Soc. Symp. Proc. **536**, 245 (1999).
[6] Z. Hassan, K. Ibrahim, M. E. Kordesch, W. Halverson, and P. C. Cloter, Int. J. Mod. Phys. B **16**, 1086 (2002).
[7] A. Al-Zouhbi and N. S. Al-din, Opt. Rev. **15**, 251 (2008).
[8] A. Bittar, H. J. Trodahl, N. T. Kemp, and A. Markwitz, Appl. Phys. Lett. **78**, 619 (2001).
[9] T. Kawashima, H. Yoshikawa, S. Adachi, S. Fuke, and K. Ohtsuka, J. Appl. Phys. **82**, 3528 (1997).
[10] P. Stumm and D. A. Drabold, Phys. Rev. Lett. **79**, 677 (1997).
[11] A. A. Demkov, J. Ortega, O. F. Sankey, and M. P. Grumbach, Phys. Rev. B **52**, 1618 (1995).
[12] O. F. Sankey and D. J. Niklewski, Phys. Rev. B **40**, 3979 (1989); O. F. Sankey, D. A. Drabold, and G. B. Adams, Bull. Am. Phys. Soc. **36**, 924 (1991).
[13] M. Ishimaru, Y. Zhang, and W. J. Weber, J. Appl. Phys. **106**, 053513 (2009).
[14] J. Nord, K. Nordlund, and J. Keinonen, Phys. Rev. B. **68**, 184104 (2003).
[15] D. A. Drabold, Eur. Phys. J. B **68**, 1 (2009).
[16] G. Kresse and J. Hafner, Phys. Rev. B **47**, 558 (1993); **49**, 14251, (1994); G. Kresse and J. Furthmüler, Comput. Mater. Sci. **6**, 15 (1996); G. Kresse and J. Hafner, Phys. Rev. B **54**, 11169 (1996), [http://cmp.univie.ac.at/vasp/]
[17] J. P. Perdew and A. Zunger, Phys. Rev. B **23**, 5048 (1981).
[18] D. Vanderbilt, Phys. Rev. B **41**, 7892 (1990); G. Kresse and J. Hafner, J. Phys. Condens. Matter **6**, 8245 (1994).
[19] B. Cai and D. A. Drabold, Phys. Rev. B. **79**, 195204 (2009).
[20] N. Mousseau and G. T. Barkema, J. Phys. Condens. Matter **16**, S5183 (2004).
[21] J. P. Perdew, K. Burke, and M. Ernzerhof, Phys. Rev. Lett. **77**, 3865 (1996); **78**, 1396 (1997).
[22] M. Yu and D. A. Drabold, Solid State Commun. **108**, 413 (1998).
[23] D. N. Talwar, D. Sofranko, C. Mooney, and S. Tallo, Mater. Sci. Eng. B **90**, 269 (2002).
[24] J. C. Nipko, C. K. Loong, C. M. Balkas, and R. F. Davis, Appl. Phys. Lett. **73**, 34 (1998).
[25] W. Pollard, J. Non-Cryst. Solids **283**, 203 (2001).
[26] Y. Pan, F. Inam, M. Zhang, and D. A. Drabold, Phys. Rev. Lett. **100**, 206403 (2008).
[27] S. Kobayashi, S. Nonomura, T. Ohmori, K. Abe, S. Hirata, T. Uno, T. Gotoh, S. Nitta, and S. Kobayashi, Appl. Surf. Sci. **113-114**, 480 (1997).
[28] B. Cai, S. R. Elliott, and D. A. Drabold, Appl. Phys. Lett. **97**, 191908 (2010).
[29] R. Atta-Fynn, P. Biswas, and D. A. Drabold, Phys. Rev. B. **69**, 245204 (2004).
[30] J. Robertson, J. Non-Cryst. Solids **354**, 2791 (2008).
[31] F. Inam, J. P. Lewis, and D. A. Drabold, Phys. Status Solidi A **207**, 599 (2010).
[32] Y.-H. Kwon, S. K. Shee, G. H. Gainer, G. H. Park, S. J. Hwang, and J. J. Song, Appl. Phys. Lett. **76**, 840 (2000).
[33] C. G. Van de Walle, C. Stampfl, and J. Neugebauer, J. Cryst. Growth **189-190**, 505 (1998).
[34] For example, B. Cai, X. Zhang, and D. A. Drabold, Phys. Rev. B **83**, 092202 (2011).